ANNUAL REVIEWS

Annual Review of Materials Research

Molecular Magnetism

Nicholas F. Chilton

Department of Chemistry, The University of Manchester, Manchester, United Kingdom; email: nicholas.chilton@manchester.ac.uk

Annu. Rev. Mater. Res. 2022. 52:79–101

First published as a Review in Advance on March 18, 2022

The *Annual Review of Materials Research* is online at matsci.annualreviews.org

https://doi.org/10.1146/annurev-matsci-081420-042553

Keywords

magnetism, chemistry, qubits, coherence, electronic structure, spin–phonon coupling

Abstract

Molecular magnetism, though distinctly a field within chemistry, encompasses much more than synthesis and has strong links with other disciplines across the physical sciences. Research goals in this area are currently dominated by magnetic memory and quantum information processing but extend in other directions toward medical diagnostics and catalysis. This review focuses on two popular subtopics, single-molecule magnetism and molecular spin qubits, outlining their design and study and some of the latest outstanding results in the field. The above topics are complemented by an overview of pertinent electronic structure methods and, in a look towards the future, an overview of the state of the art in measurement and modeling of molecular spin–phonon coupling.

1. INTRODUCTION

The field of molecular magnetism concerns the study of paramagnetic molecule-based materials and is a fantastic playground for chemists, physicists, materials scientists, experimentalists, and theorists to explore. The great appeal of these materials is the tunability of their magnetism via chemistry, where the connection between structure and physical properties can be modulated in practically infinite ways, a significant difference from solid-state magnetic materials. Further, the inherent locality of molecular magnetic moments allows the simulation of magnetic states with Hamiltonians of finite dimension, facilitating the exact treatment of quantum magnetic properties. The combination of these two features allows the precise construction of magnetic topologies to study fundamental physics. For instance, slow magnetic dynamics can be engineered in zero-dimensional (0D) single-molecule magnets (SMMs), which are atomically precise superparamagnets with tunable magnetic anisotropy (1); low-dimensional magnetism can be studied in 1D single-chain magnets (2) or in 2D layered materials (3); the quantum–classical boundary can be studied with large spin clusters (4); optical-, thermal-, or pressure-induced spin state switching can be studied in spin-crossover (SCO) materials (5); magnetic frustration [both Heisenberg (6) and Ising (7) models] and toroidal spin textures (8) can be studied in cyclic molecules; spin waves can be studied in larger cyclic molecules (9, 10); and coherent spin dynamics can be manipulated in molecular spin qubits (11, 12). Beyond an interest in controlling and studying the fundamental physics of tailored magnetic systems, molecular magnets are often touted for their potential in high-density data storage (13), quantum information processing (14), and spintronics (15) and are central in the design of multimodal magnetic resonance imaging (MRI) contrast agents (16). This review does not dwell on applications, save one exception: highlighting a recent paper showing the potential of molecule-based magnets. Oyarzabal, Clérac and coworkers have recently studied the deceptively simple $[CrCl_2(pyrazine)_2]$ coordination polymer, a 2D ferrimagnet consisting of localized Cr(III) sites with a mixed-valent pair of pyrazine ligands (3), and shown that it can be reduced to make a new 2D framework, $Li_{0.7}[Cr(pyrazine)_4]Cl_{0.7}\bullet 0.25THF$, which features localized Cr(II) sites and pyrazine radical spins and shows ferrimagnetic ordering up to 510 K and a coercive field of 0.75 T at 300 K (17). This is an incredible set of properties for a magnet with a density of ~1.3 g/cm^3 compared to solid-state alloys which are far denser, such as neodymium ($Nd_2Fe_{14}B$, ~7.5 g/cm^3), samarium-cobalt ($SmCo_5$, ~8.3 g/cm^3), AlNiCo (~7 g/cm^3), or ferrite (~5 g/cm^3) magnets, and that can also potentially be exfoliated and used as a 2D magnet.

Sections 2 and 3 deal with the specific cases of SMMs and molecular qubits, respectively, which encapsulate a great deal of research in the field. Section 4 then gives an overview of the relevant electronic structure theories pertaining to metal ions in molecular magnets. Finally, Section 5 discusses the crucial importance of the spin–phonon interaction before concluding with an outlook on the field in Section 6.

2. SINGLE-MOLECULE MAGNETS

The identification of large magnetic anisotropy in $[Mn_{12}O_{12}(CH_3COO)_{16}(H_2O)_4]$ [herein $\{Mn_{12}\}$] (18) led to the first observation of molecular magnetic hysteresis and the definition of SMMs (19, 20): molecules that show memory effects arising from purely intramolecular interactions without the need for long-range order. As such, these 0D magnetic materials have no phase transitions and are technically superparamagnets. This report sparked an intense investigation over the subsequent 30 years to find SMMs with slower magnetic dynamics in the hope of realizing molecule-based high-density magnetic memory (21). The crucial ingredients for SMMs were clearly laid out: (*a*) a large magnetic moment, (*b*) a bistable ground state, and (*c*) large easy-axis magnetic anisotropy. The first two points are rather self-explanatory: a very magnetic molecule is required to make a molecular magnet, and classical binary memory requires two degenerate states

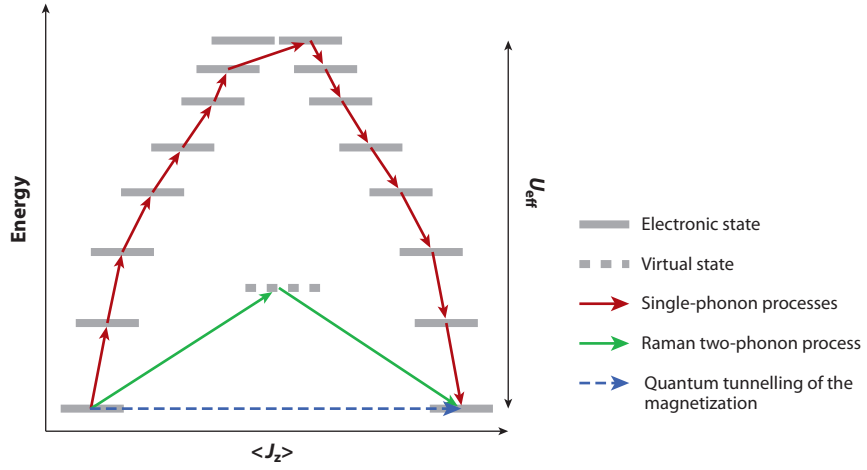

Figure 1

Illustrative energy barrier to magnetic relaxation (U_{eff}) in single-molecule magnets. Gray bars are doubly degenerate electronic states (Kramers doublets), which have opposite projections of the total angular momentum J_z. Magnetic relaxation processes mediated by phonons are shown as colored solid arrows, with red indicating single-phonon processes (the sequence displayed is called the Orbach process) and green indicating a Raman two-phonon process. The gray dashed line indicates a virtual state, which is not a real state and simply depicts that all excited states are involved in a second-order perturbation to facilitate the Raman-like scattering process. Magnetic relaxation mediated by quantum tunneling of the magnetization is shown as a blue dotted arrow. Thermally assisted quantum tunneling of the magnetization between excited states is not shown.

that can be switched between. The third requirement is perhaps the most crucial and yet the trickiest component to engineer. Magnetic anisotropy is the connection between the physical structure of a molecule and its magnetic properties, and uniaxial easy-axis anisotropy dictates that a single spatial direction should have the largest magnetic susceptibility. This set of properties engenders a well-isolated manifold of magnetic states that display a characteristic shape (**Figure 1**), where an intrinsic energy barrier separates a doubly degenerate ground state that each molecule should climb in order to reverse its magnetization; this is the origin of slow magnetic dynamics, and hence memory effects, in SMMs. This energy barrier to magnetic reversal (or magnetic relaxation) is given the symbol U_{eff} and leads to an exponential temperature dependence of the magnetic relaxation rate, which is also called the spin-lattice relaxation rate (T_1), as shown in Equation 1 (22),

$$\tau^{-1} = \tau_0{}^{-1} e^{-U_{eff}/k_B T}. \quad 1.$$

This is similar to the Arrhenius law for chemical kinetics; for $\{Mn_{12}\}$, $U_{eff}/k_B = 61$ K, and hysteresis is observable below 4 K. However, as magnetic relaxation involves the exchange of energy with a bath, nearly any paramagnetic molecule can show out-of-equilibrium behavior (i.e., memory effects) if the temperature is low enough and the timescale of the experiment is short enough. Hence, while it is commonplace to refer to any molecule with observable slow magnetic dynamics as an SMM, the author prefers a definition that includes the presence of a U_{eff} barrier.

The initial area of interest for the development of SMMs was 3d-based polymetallic molecules in the vein of $\{Mn_{12}\}$, where exchange interactions were harnessed to construct molecules with giant total spin [culminating recently with $S = 91$ in a $\{Ni_{21}Gd_{20}\}$ complex (4)]. In this, the first generation of SMMs, the magnetic anisotropy and U_{eff} arise from second-order (excited state) spin-orbit coupling (SOC) effects in each of the 3d ions, which are projected onto the total spin

ground state of the molecule. Thus, while magnetic moments can be quite large due to their large total spin, the magnetic anisotropy of each ion is usually small and tends to cancel out when projected onto the total ground spin state (as controlling a collinear alignment of many individual anisotropy axes is synthetically challenging), meaning that U_{eff} values are small.

Inspired by the pioneering work of Ishikawa et al. (23), who in 2003 isolated the Tb(III) SMM $[N^nBu_4][TbPc_2]$ (H_2Pc = phthalocyanine) with $U_{eff}/k_B = 331$ K, the community turned to the use of 4f ions in SMMs, most often as monometallic complexes (24). This is because 4f ions have near-unquenched orbital angular momentum and large numbers of unpaired electrons, both of which are due to the contracted nature of the 4f orbitals, leading to large magnetic moments as well as large magnetic anisotropy. Here, SOC acts in first order to give total angular momentum $J = L + S$ ground states in the late 4f period ($J = L - S$ in the early 4f period), and owing to the contracted 4f orbitals, the crystal field (CF) effects are best described as splitting their total angular momentum states J into projections m_J. As a result, it is irrelevant to talk about 4f bonding or antibonding interactions with ligands. Thus, the U_{eff} barrier for monometallic 4f-based SMMs arises from the splitting of the ground total angular momentum state J by the CF. The requirement for magnetic bistability can also be ensured by choosing a 4f ion with an odd number of unpaired electrons, which via Kramers' theorem ensures twofold degeneracy in zero magnetic field (25). Hence, the ion of choice to build SMMs was quickly found to be Dy(III), which has a $^6H_{15/2}$ ground term. After a scattergun approach to the design of new 4f SMMs, a seminal perspective paper from Rinehart & Long (26) proposed a method for rational design of 4f-based SMMs. It is of critical importance how the effective CF of a set of ligands splits the m_J states, which at first glance is a terrifying problem to reverse engineer, but a crucial piece of the puzzle was actually solved in the 1980s by Sievers (27), who showed that the m_J states of the free 4f ions have analytical f-electron density distributions that are strongly anisotropic. Thus, Rinehart and Long proposed to arrange the electrostatic potential generated by the ligands to stabilize the anisotropic f-electron density of the largest (most magnetic) m_J state of a given 4f ion. Indeed, a classical electrostatic model was shown to match the results of ab initio electronic structure calculations of the ground state magnetic anisotropy in Dy(III) complexes (28). For Dy(III) the coordination geometry of choice is two-coordinate linear (29, 30), concentrating negative charge on a single axis (**Figure 2**), and the strategy has been validated countless times as yielding vast increases in U_{eff} barriers (**Figure 2*b***) (31).

Recently, a step change in the performance of SMMs was achieved by Goodwin et al. (32) by fully conforming to this design in the isolation of the first dysprosocenium cation $[Dy(C_5H_2{}^tBu_3)_2]^+$, which is a sandwich complex with no equatorial ligands. This is a remarkably challenging class of molecule to isolate, and numerous attempts had been made previously by Layfield and coworkers (33) as well as others (34–36). There are now five other closely related dysprosocenium SMMs (37, 38), one bis-mono-phospholyl Dy(III) SMM ($[Dy(C_4P^tBu_2Me_2)_2]^+$) (39), and one neutral terbocene SMM $[Tb(C_5{}^iPr_5)_2]$ (40), which have set the new benchmark in the research field, with U_{eff}/k_B between 1,760 and 2,217 K and open magnetic hysteresis up to 80 K (38). These findings have driven both theoretical (32, 39, 41) and experimental (42) studies to examine how and why this class of compounds has such extraordinary properties, with the conclusions being that (*a*) the ligands are small and charge dense, (*b*) the lack of equatorial ligands allows close approach of the axial ligands, (*c*) the bulky nature of substituents encourages linear coordination, (*d*) the first coordination sphere of the Dy(III) ion contains rigid C_5 (or C_4P) rings leading to high-energy intramolecular vibrations (optical phonons), and (*e*) the bulky substituents on these cations paired with bulky anions result in diffuse molecular charges, leading to weak intramolecular interactions and low-energy intermolecular vibrations (acoustic and pseudoacoustic phonons). Points *a–c* lead to a large CF splitting and hence a large U_{eff} barrier, slowing down relaxation via the Orbach mechanism (Equation 1), while *d* and *e* lead to weak two-phonon coupling, slowing

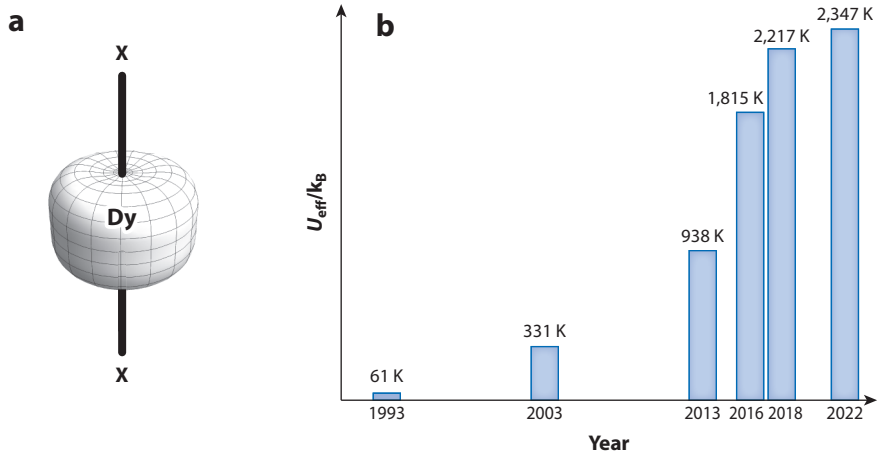

Figure 2

(*a*) The ideal coordination environment for a Dy(III)-based single-molecule magnet is linear two-coordinate. X represents anionic ligand donor atom(s), and the rendered shape is the overexaggerated $4f^9$ electron density for Dy(III) in the $m_J = \pm 15/2$ state (27). (*b*) Timeline of record-breaking U_{eff} barriers for different SMMs: 1993, $[Mn_{12}O_{12}(CH_3COO)_{16}(H_2O)_4]$ (43); 2003, $[N^nBu_4][TbPc_2]$ (23); 2013, [TbPc(Pc-(OPh-*p*-^{t}Bu)$_8$)] (44); 2016, $[Dy(O^tBu)_2(pyridine)_5][B(C_6H_5)_4]$ (45); 2018, $[Dy(C_5Me_5)(C_5{}^iPr_5)][B(C_6F_5)_4]$ (38); and 2022, $[Dy_2I_3(C_5{}^iPr_5)_2]$ (46).

down relaxation via the Raman mechanism (see below) (42). How to improve on this design is an open challenge, and theoretical research suggests that U_{eff} barriers have reached their maximum, but that progress can be made by judiciously designing the vibrational modes of the SMM (41).

Indeed, other SMMs with similarly large U_{eff} barriers do not show open hysteresis to such high temperatures (31, 47); this is because magnetic relaxation does not follow an exponential temperature dependence in all temperature ranges. Magnetic relaxation, whereby molecules move between different electronic states, is facilitated by absorption and emission of phonons (see Section 5). The exponential over barrier process (Orbach process) arises from a concatenated series of single spin–phonon processes, but there are also Raman-like two-phonon scattering processes, which give a power-law temperature dependence to the relaxation rate (25, 48), and quantum tunneling of the magnetization (QTM), which is temperature independent (49, 50), both of which allow for shortcutting of the U_{eff} barrier (**Figure 1**). Thus, two of the most significant areas in the development of SMMs are (*a*) unraveling the connection between Raman relaxation and chemical structure and (*b*) understanding the drivers of QTM in 4f SMMs. These goals are strongly intertwined with theory, as discussed further in Section 5.

Through the work on monometallic 4f SMMs that now dominates the field, it has become well known how to design molecules that exhibit large magnetic anisotropy. However, progress is not sure to continue along this route owing to fundamental limitations in the possible chemistry and the underlying physics. Another route to improving the performance of SMMs is through strong magnetic coupling between 4f ions, which can augment existing strong anisotropy. However, magnetic interactions between 4f ions are generally weak and often dominated by through-space dipolar interactions (51); hence, polymetallic 4f molecules tend to behave magnetically as a collection of individual 4f centers (52). However, strong interactions can be effected by the inclusion of radical spins on suitable bridging ligands, leading to strong 4f–4f coupling (53). Here, the most emblematic example is $[\{Tb(tetrahydrofuran)(N\{SiMe_3\}_2)_2\}_2N_2]$, which features a bridging N_2^{3-} radical anion having strong antiferromagnetic coupling to each Tb(III), leading to a highly

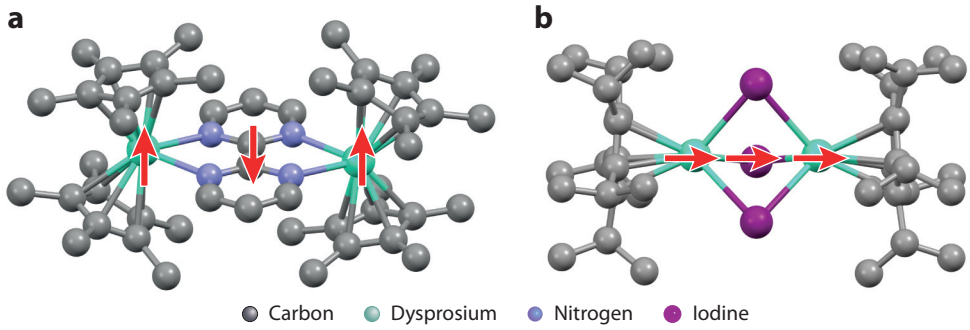

Figure 3

Chemical structures of (*a*) $[(Dy(C_5Me_5)_2)_2(bipyrimidine)]^+$ (58) and (*b*) $[Dy_2I_3(C5^iPr_5)_2]$ (46) with indication of anisotropic magnetic moments in the ground state (*red arrows*). H atoms are omitted for clarity.

anisotropic ferrimagnetic ground state (54). This molecule held the record for the highest temperature observation of molecular magnetic hysteresis, 14 K, until the advent of dysprosocenium SMMs (32), but crucially, these strongly coupled SMMs feature large coercivities (55) that appear to block the effects of QTM that plague monometallic 4f SMMs (56, 57). However, most of these radical-bridged SMMs feature anionic radical bridging ligands that coordinate in a perpendicular fashion to the main anisotropy axis of each of the metal ions (**Figure 3*a***) (55, 58, 59); it would be preferable if the radical bridge was collinear with the local anisotropy axes such that (*a*) any coupling between the metal ions was supported by through-space ferromagnetic dipolar interactions and (*b*) the anionic radical bridge enhanced, rather than detracted from, the existing magnetic anisotropy (**Figure 3**). An intriguing development in this area has been the advent of dimeric 4f units encapsulated by fullerene cages that exhibit single-electron metal–metal bonds that engender very strong magnetic coupling (60). Here, the bonding electron is both the source of the anisotropy for each Dy(III) ion (negative charge on a single axis) and the source of magnetic coupling, which, importantly, follows the collinear principle. This leads to an order-of-magnitude stronger interaction than usually observed (even for radical-bridged complexes) and magnetic hysteresis open up to 21 K.

Taking inspiration from this idea, Chilton, Harvey, Long, and coworkers (46) have recently isolated a series of dimetallic 4f complexes $[Ln_2I_3(C_5{}^iPr_5)_2]$ (Ln = Gd, Tb, Dy) featuring a stable single-electron bond that is collinear with the local anisotropy axes (**Figure 3*b***). The extra electron resides in a σ-bonding $5d_z{}^2$–$5d_z{}^2$ orbital, and hence each Ln ion has a formal valence of +2.5 and the molecules are Robin–Day class III mixed valent. These remarkable molecules exhibit incredibly strong 4f–radical coupling (another order of magnitude stronger than the fullerene-encapsulated dimers), shown to be dominated by direct exchange, and CF splitting larger than the best monometallic SMM $[Dy(C_5Me_5)(C_5{}^iPr_5)][B(C_6F_5)_4]$. These two features, including significant exchange anisotropy, result in the highest U_{eff} barrier to date for $[Dy_2I_3(C_5{}^iPr_5)_2]$ with $U_{eff}/k_B = 2{,}347$ K, open magnetic hysteresis up to 80 K, and a coercive field $\geq$14 T at 60 K (preliminary measurements estimate a coercive field $\geq$25 T at 50 K for $[Tb_2I_3(C_5{}^iPr_5)_2]$); for comparison, the coercive field of $[Dy(C_5Me_5)(C_5{}^iPr_5)][B(C_6F_5)_4]$ at 60 K is 2.1 T.

3. MOLECULAR QUBITS

Given the quantum origins of magnetism in molecules, it is no surprise that these materials have found applications in quantum information processing. The fundamental unit of quantum

computing is the qubit: an entity that has a well-defined two-level quantum system that can be manipulated and retains phase coherence; the conditions for ideal qubits are laid out by the DiVincenzo criteria (61). In the case of magnetic molecules, a qubit could be constructed on the basis of the electron and/or nuclear spins, where the simplest incarnation could be a V(IV) or Cu(II) complex with one unpaired electron, and the $m_S = \pm 1/2$ states form the two-level basis. Candidate qubits must first demonstrate that arbitrary superposition states can be formed, that is, $|\psi\rangle = \alpha|+1/2\rangle + \beta|-1/2\rangle$, and that the phase coherence remains long enough to be practically useful. In the realm of molecular qubits, manipulation is dominated by pulsed electron paramagnetic resonance (EPR) spectroscopy, where the spin-echo coherence time T_2 of a qubit can be measured with pulsed EPR using a Hahn echo sequence (62). This ubiquitous pulse sequence usually employs a train of 16 ns microwave pulses to (*a*) flip the magnetization by 90° ($\pi/2$ pulse) from being aligned with the field (z) to being perpendicular to it (x), (*b*) allow the magnetization to freely precess in the field and individual components in the ensemble to dephase, (*c*) flip the magnetization by 180° (π pulse), and (*d*) allow the magnetization to precess back together and record the spin echo (along $-$x). Demonstration of coherent manipulation is routinely shown by performing a nutation experiment, where the result is Rabi oscillations of the magnetization. Modern spectrometers employ arbitrary waveform generators to generate pulses of arbitrary shape with subnanosecond resolution, allowing specific pulses that could excite a precise subpopulation in the ensemble or a broadband pulse to excite the whole sample, for example. The best-performing molecular qubits show spin-echo coherence times on the order of a microsecond at room temperature (63–65) and up to almost a millisecond at low temperatures (66) compared to their solid-state rivals with spin-echo coherence times of a few milliseconds at room temperature for negative nitrogen vacancy (NV^-) defects (67) or up to tens of milliseconds for silicon carbide divacancy defects when driven appropriately at low temperatures (68). Despite the coherence times of molecular qubits being 10–1,000 times shorter than solid-state alternatives, this is no barrier to utility given that gate operations issued by microwave pulses are on the order of nanoseconds.

It must be mentioned here, however, that nearly all experiments on molecular qubits are conducted on ensembles and not individual molecules; the initialization, manipulation, and detection of a single molecular spin is a significant challenge, but not one that is impossible. Given this difficulty, the question "Why molecular spin qubits?" is pertinent. The answer lies in a basic tenet of chemistry: A sample of a pure compound contains a very large number ($\sim 10^{23}$) of identical molecules that are prepared simultaneously. This gives molecular qubits a cost and time advantage in their preparation if the difficulties with their use can be addressed. Chemical synthesis also offers a unique angle for the preparation of more than just two-level systems. Arrays of weakly interacting two-level systems can be constructed in arbitrary architectures (69, 70), including into infinite arrays (71–73), and multilevel electronic or nuclear systems can be incorporated (74) to develop simple gates (75–77) and implement error-correction schemes (78). Hence, the near-infinite tunability of chemical synthesis can be brought to bear on the degrees of freedom of molecular qubits, which cannot be said about impurity spins in the solid state or fabrications of superconducting circuits. Moreover, in the realm of quantum sensing, molecules are far more susceptible to changes in their environment than solid-state impurities or trapped ions, and hence there is certainly optimism about the role of molecular qubits in the broader space of quantum information (79, 80).

Many of the challenges associated with the utility of molecular qubits are highlighted when they are compared with their solid-state counterparts; however, possible solutions to these challenges can also be taken from the solid state. For instance, the explosion in utility of NV^- centers (81) is enabled by optical initialization and readout, a strategy that is very hard to conceive of in a molecular analog. However, a molecular spin qubit that can be initialized and read out with

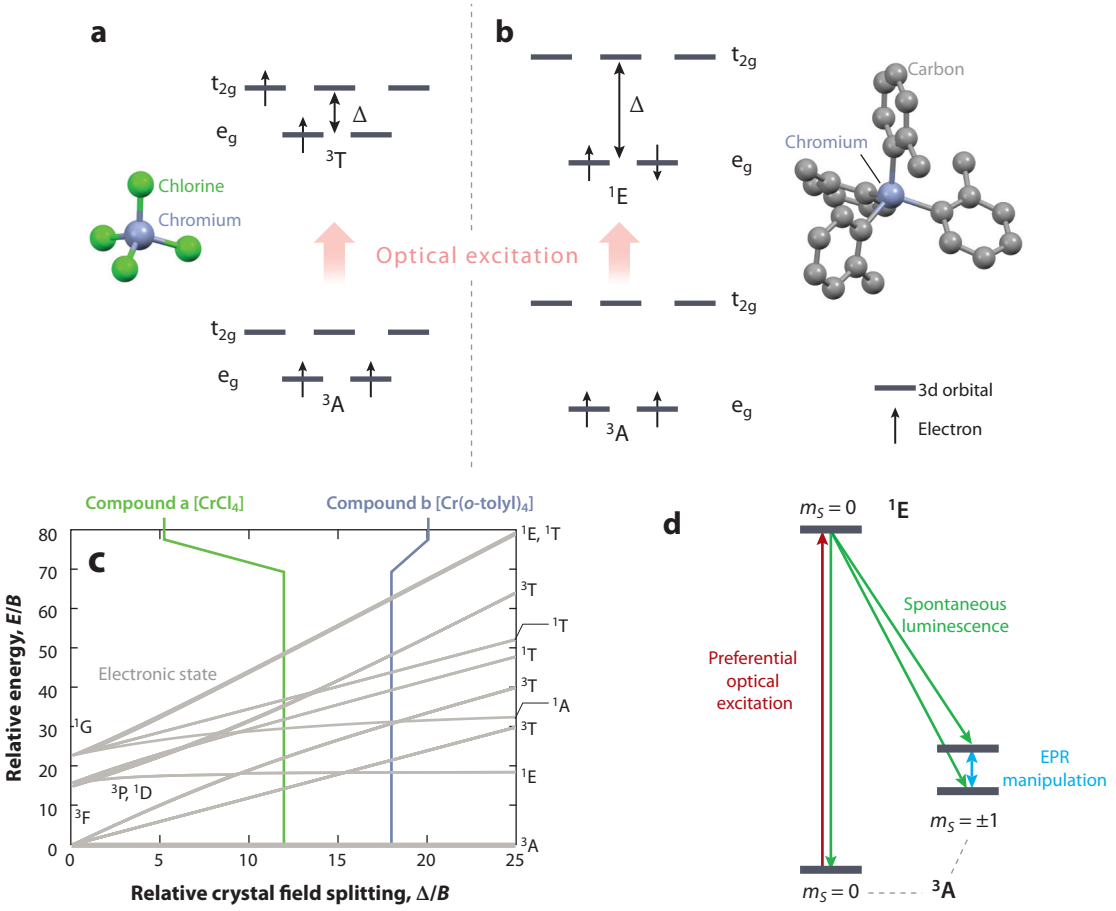

Figure 4

(*a*) Weak tetrahedral crystal field splitting (Δ) of 3d orbitals in $[CrCl_4]$ into lower-lying e_g set and higher-lying t_{2g} set, with ground ^3A term and first excited ^3T term. (*b*) Strong tetrahedral crystal field splitting in $[Cr(o\text{-tolyl})_4]$ (H atoms omitted for clarity) leading to ground ^3A term and first excited ^1E term. (*c*) Tanabe–Sugano diagram for the d^2 configuration in tetrahedral symmetry with Racah parameter $C/B = 5.25$; ^1S atomic state and its corresponding ^1A crystal field state are not shown. (*d*) Optical excitation and emission pathways and qubit manipulation with electron paramagnetic resonance (EPR) for $[Cr(o\text{-tolyl})_4]$, as determined in Reference 91.

light has recently been reported by Freedman, Awschalom, and coworkers (82), who show that $[Cr(o\text{-tolyl})_4]$ has the requisite spin structure to permit such operations in a molecule. The key design features are that Cr(IV) is in a tetrahedral environment, assuring an $S = 1$ ground state for the d^2 configuration with small magnetic anisotropy (**Figure 4*a*,*b***), and that aryl carbon ligands impose a very strong CF, enforcing an $S = 0$ first excited state (**Figure 4*b***). Here, the design parameter is the strength of the CF relative to the interelectronic repulsion, which is neatly expressed with the appropriate Tanabe-Sugano diagram (**Figure 4*c***), showing that the tetrahedral CF must be approximately three times larger than the Racah C parameter (83) in order to achieve the desired spin state ordering. This strong-field electronic structure facilitates preferential optical excitation from the $m_S = 0$ state in the ground $S = 1$ manifold to the excited $S = 0$ state, and so population becomes trapped via luminescence in the dark $m_S = \pm 1$ states (**Figure 4*d***); similar strategies are possible with V(III) complexes (84). In a similar vein, Coronado, Hill,

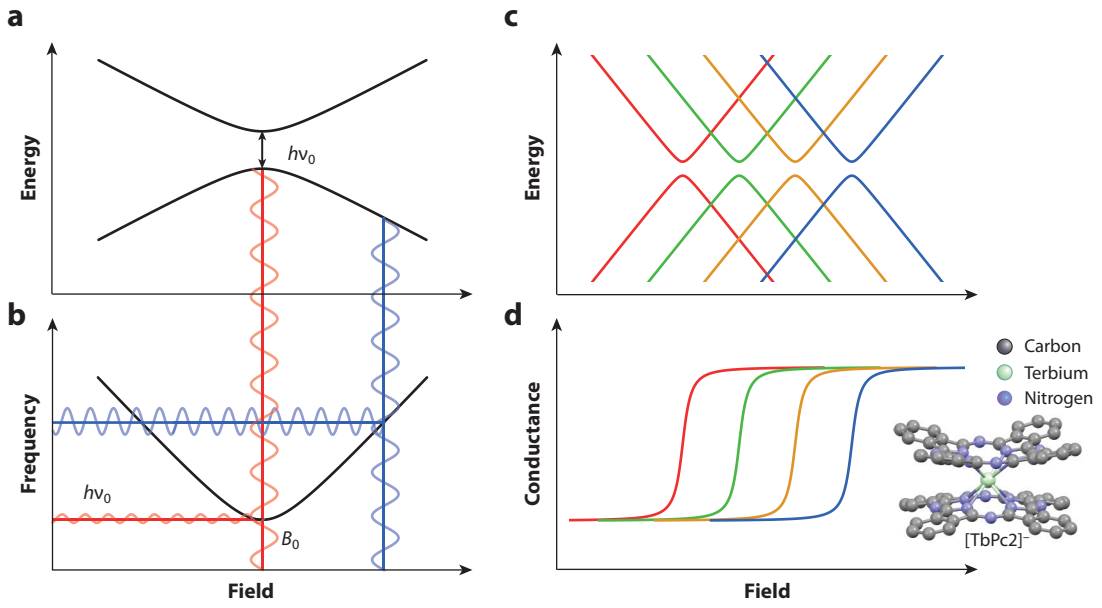

Figure 5

(*a*,*b*) Schematic of an avoided crossing in $Na_9[Ho(W_5O_{18})_2]$ leading to clock-like protected electron paramagnetic resonance (EPR) transitions, as explained in Reference 92. Vertical oscillations indicate longitudinal magnetic field noise, leading to small changes in the EPR transition frequency at the clock transition (*red*) or large changes off the clock point (*blue*). (*c*) Schematic of electron–nuclear avoided crossings of $[TbPc_2]$, as explained in Reference 93. The colored lines represent the different nuclear spin projections of $I = 3/2$ for ^{159}Tb. (*d*) Schematic of conductance jumps in $[TbPc_2]$ owing to quantum tunneling of the magnetization at avoided crossings. The colored lines show the conductance measured when the molecule is in each of the corresponding nuclear spin states in panel *c*. The inset shows the molecular structure of $[TbPc_2]^-$ (99).

and coworkers (85) have taken inspiration from atomic physics, where protected atomic clock transitions lead to ultrastable and sharp spectroscopic lines (86), to develop molecular qubits with orders-of-magnitude enhancement in spin-echo coherence times at electron-nuclear hyperfine avoided crossings in a Ho(III) molecular qubit, $Na_9[Ho(W_5O_{18})_2]$. Here, the ground state is $m_J = \pm 4$, arising from a CF of near-D_{4d} symmetry acting on the $^5I_8$ ground term. However, the ground state is not perfectly degenerate because the ion has an even spin, $S = 2$, and thus is non-Kramers; hence, the low-symmetry component of the CF can completely remove the electronic degeneracy in zero field. In this case, the leading CF term lower than D_{4d} symmetry has fourfold rotational symmetry and thus mixes the $m_J = \pm 4$ with each other in second order, leading to an unusually large avoided crossing at zero field ($\sim$0.3 cm^{-1}; **Figure 5*a***). This avoided crossing results in an EPR transition frequency that is insensitive to longitudinal magnetic field noise at first order (**Figure 5*b***), and hence the two-level system is protected against decoherence from such sources when operated at this clock point. In reality, the ^{165}Ho isotope has $I = 7/2$ and so there are actually eight avoided crossings, one for each projection of the nuclear spin m_I. Even more recently, the team has also demonstrated this effect in a Lu(III) molecular qubit (87). When operated at the clock points, it becomes the spin-lattice T_1 time that begins to limit the phase memory of molecular qubits, and hence the same questions of spin–phonon engineering arise as for SMMs. In this respect, Atzori, Sessoli, Salvadori, and coworkers (88–90) have made important contributions in probing spin dynamics and vibrations in vanadyl(IV) molecular qubits, demonstrating the link between molecular rigidity and improved T_1 and T_2 times.

However, to date, there has been only one successful demonstration of a complete quantum algorithm using a single molecule spin qubit processor, with the pace being set by Candini, Ruben, Wernsdorfer, Balestro, and coworkers (94–98). Here, the team has long favored the use of the first 4f SMM, $[TbPc_2]^-$ (23); this molecule features large uniaxial easy axis magnetic anisotropy imposed by the CF on the $^7F_6$ ground term of Tb(III), leading to a near-degenerate pair of $m_J = \pm 6$ ground states. Similar to $Na_9[Ho(W_5O_{18})_2]$, the ground state is not degenerate because Tb(III) is a non-Kramers ion, and here the avoided crossing at zero field (**Figure 5*a***) facilitates QTM when the field is swept through zero. This abrupt reversal of magnetization via QTM leads to a measurable change in the conductivity of the molecule when placed on a graphene nanoribbon (94) or carbon nanotube (95), and thus the magnetization of the sample can be measured via conductance. However, there is a single stable isotope, ^{159}Tb, which has nuclear spin $I = 3/2$, and hence there are actually four avoided crossings at different field positions owing to the hyperfine coupling (**Figure 5*c***), meaning that conductance measurements of a single molecule in a gold break junction allow measurement of the projection m_I of a single nuclear spin (**Figure 5*d***) (93). Thus, the nuclear spin of this molecule can be initialized in a particular m_I state by sweeping the magnetic field and then coherently manipulated with microwaves (97), allowing for the demonstration of the Grover search algorithm in a single molecular qubit (98).

4. ELECTRONIC STRUCTURE AND MODELING OF MOLECULAR MAGNETS

For most contexts in molecular magnetism, it is sufficient to consider metal ions as gas-phase ions perturbed by a molecular environment (i.e., an ionic bonding model as opposed to a covalent one). This simplification can break down in cases of strong metal–ligand bonding [e.g., organometallic compounds such as ferrocene (100)], significant metal–metal interactions [e.g., mixed-valence chemistry (101)], incorporation of redox noninnocent character [e.g., Ce(III)/Ce(IV) complexes (102, 103)], and low-valent complexes [e.g., divalent 4f-block chemistry (104, 105)]; however, it is usually still a good starting point for understanding magnetic properties.

Under the single-configuration approximation of gas-phase metal ions, the leading perturbations removing the degeneracy of d^n or f^n configurations are interelectron repulsion (IER) and SOC. The latter, being a relativistic effect, becomes more significant for heavier elements, but even for the 3d metals it gives rise to many interesting properties in molecular magnetism. The parametric models of atomic and ionic electronic structure as developed by Slater (106) and Condon (107) [and later developed in spherical tensor mathematical form by Racah (108, 109)] provide convenient tools to model the electronic energy levels owing to these perturbations. These methods allow the classification of states by their Russell-Saunders terms, defined by total spin quantum number S, total orbital angular momentum quantum number L, and total angular momentum quantum number J; in spectroscopic notation, this is $^{2S+1}L_J$. When incorporated into molecular complexes, it is usually assumed that the IER and SOC are more-or-less unchanged and the main perturbation to the metal ion is the loss of degeneracy of the d- or f-orbitals. In reality, this is due to the formation of molecular orbitals, but in an ionic metal-ion-centric picture this is often described in terms of CF or ligand field (LF) theory. The distinction between CF and LF theories is largely a matter of definitions; the original CF theory described by Bethe (110) assumed a purely ionic model where perturbations to the free-ion electronic structure were caused by point-charge electrostatics, while LF theory accounts for the formation of bonding/antibonding orbital interactions in molecular complexes (111), along with corrections for polarization, screening, orthogonality, etc. (112). However, in modern research it is understood that any description of the environment of a metal ion, whether in a molecular complex or a solid-state impurity, in terms of

a symmetry-adapted expansion acting on a basis of metal angular momentum functions, such as in Equation 2,

$$\hat{H}_{\mathrm{CF}} = \sum_{2 \le k \le 2J}^{\text{even}} \sum_{q=-k}^{k} B_k^q \hat{O}_k^q, \qquad 2.$$

is purely phenomenological. Hence, we are agnostic as to the distinction between CF and LF formalisms and happily use them synonymously. The CF potential can be written in terms of the single-electron orbital angular momentum functions of the microstate basis *l*, the total orbital angular momentum states *L*, or the total angular momentum basis *J*, and most commonly the extended Stevens operators ($\hat{O}_k^q$, based on the tesseral harmonics) are employed (113). These operators are also closely related to those used to describe the effective zero-field splitting (ZFS) of spin-only states measured with EPR spectroscopy, but care must be taken to avoid confusion between conventions and the two rather different electronic structure paradigms (114).

The confluence of these three components of metal-ion electronic structure—IER, SOC, and CF—compete to dictate the magnetic properties of a molecular complex and allow the grouping of different blocks of the periodic table into different classes. For 3d ions where IER $\sim$ CF $\gg$ SOC, it is vitally important to understand the 3d orbital energies and ordering that lead to a particular electronic ground state before the importance of SOC can be considered. For instance, 3d complexes often have quenched orbital angular momentum in the ground state so that SOC is a minor perturbation (but care must be taken in specific cases; e.g., a weak octahedral CF for $3d^7$ gives a triply degenerate orbital ground state and hence non-zero orbital angular momentum). In contrast, for the 4f ions where IER > SOC > CF, 4f orbital splitting is more-or-less irrelevant, and it is usually the ground Russell-Saunders total angular momentum term $^{2S+1}L_J$ that the CF is considered to split. For other metal ions in the periodic table, IER $\sim$ CF $\sim$ SOC, and so the electronic structure is not trivial and must be considered on a case-by-case basis.

Measurement of the magnetic moment of transition metal complexes in addition to optical absorption spectroscopy provides information on the coordination geometry and CF splitting of the metal ions and forms the cornerstone of inorganic chemistry experiments in many undergraduate programs. While experimental characterization of molecular magnets by thermodynamic and spectroscopic measurements provides crucial data, they can be insufficient on their own to fully characterize the electronic states; the data may not be complete, they may not have sufficient resolution, or perhaps samples are not amenable to some techniques. Hence, in modern research, physical measurements of molecular magnets are usually accompanied by a quantum mechanical model to reproduce and hence explain the experimental data; the most powerful models are the simplest models that can reproduce all observables. These often take the form of model Hamiltonians, where the choice of basis (e.g., full configuration d^n or f^n microstate basis, CF term, Russell-Saunders term, or pseudospin ground state) depends on the experimental data available. The golden rule is to model only the states that can be observed, as the bigger the model, the more parameters that require data to be well defined. For instance, in low-temperature EPR experiments where only the lowest states within a few wavenumbers are detected, only the ground spin state or lowest Kramers doublet is required; in the case of 4f luminescence spectroscopy where many different excited terms are observed, an f^n microstate basis is mandated. Many excellent software packages are available nowadays for performing such analyses, such as EasySpin (115), CONDON (116), and PHI (117).

In many cases, such phenomenological models are an excellent means of comparing different molecular magnets and explaining differences via transferrable model parameters. However, there are cases where even the simplest of such models are vastly overparameterized, and a multitude of different parameterizations provide adequate fits to experimental data. For example,

one could build a model CF Hamiltonian acting on the ground Russell-Saunders term to model the magnetic properties of a 4f ion in a molecule; however, in cases of low symmetry (which form the overwhelming majority of molecular magnets), such a model would have a minimum of 26 CF parameters (112). Even with optical spectroscopy, EPR, and magnetic data, the parameter space is so large that it is impractical to find the true parameterization. Hence, these days it is commonplace that a full characterization of a molecular magnet includes some form of ab initio computation to provide estimates for, or validation of, model parameters. The calculation of the electronic structure and magnetic properties of metal complexes is not a trivial exercise; one must accommodate the strong electron correlation in metal ions while incorporating excited states and accounting for spin–orbit coupling, all in the presence of often large and low-symmetry organic ligands. While density-functional theory (DFT) remains the gold standard in the solid state, it is a single-configurational theory and hence is unable to describe the first-order static correlation of near-degenerate d- or f-orbitals with unequal occupations. However, given the intrinsic finite nature of molecules, relatively high levels of theory are amenable to treating such problems, and complete active space self-consistent field (CASSCF) (118) calculations have emerged as the de facto standard for approximating the magnetic properties of molecules (119). CASSCF is a multiconfigurational method that allows direct treatment of the strong electron correlation present in metal ions and is usually performed with a relativistic approximation accounting for scalar effects at the spin-free level with SOC included a posteriori, often termed CASSCF-SO. This method requires definition of an active space of molecular orbitals in which electron correlation effects are exactly determined, which leads to its utility in the calculation of magnetic properties of metal complexes where the definition of the active space can be as simple as the d- or f-orbitals (of course, more advanced treatments require more than this minimal active space). Hence, there is no need for empirical corrections, such as the popular DFT+U Hubbard model (120, 121), in CASSCF-SO. However, it is important to note that electron correlation for the fully occupied and unoccupied molecular orbitals is completely absent (these electrons are essentially treated with Hartree-Fock theory), and hence CASSCF methods do not account for the important effects of dynamic correlation (122). It is for these reasons that DFT methods, where electron correlation is approximated, are still very useful for structural properties in cases without critical strong correlation effects [e.g., diamagnetic or spin-only complexes such as Mn(II), Fe(III), Gd(III), and octahedral Cr(III)]. The effects of dynamic correlation can be included in CASSCF methods via perturbative approaches such as CASPT2 (123) or NEVPT2 (124); however, these are very demanding calculations that have their own shortcomings and difficulties and so are often omitted in the molecular magnetism community. Nonetheless, the basic CASSCF-SO method usually provides accurate enough results to verify experimental results or provide a good starting guess for model parameters.

5. SPIN–PHONON INTERACTIONS

Spin–phonon interactions are important throughout molecular magnetism because they lead to loss of memory in SMMs and contribute to loss of phase coherence in molecular qubits, among other things, but understanding these interactions is very difficult. This is for several reasons: (*a*) there are lots of phonon modes in solids, (*b*) spin–phonon interactions are hard to measure, and (*c*) these interactions are hard to calculate. Various techniques can be employed to address the first challenge, that is, experimental characterization of the phonon density of states (DOS). Undoubtedly the most common measurements are infrared (IR) and Raman spectroscopies; however, these are only able to probe phonon modes at the center of the first Brillouin zone (the gamma point), while phonons of all wave vectors participate in spin–phonon coupling. While also only capable

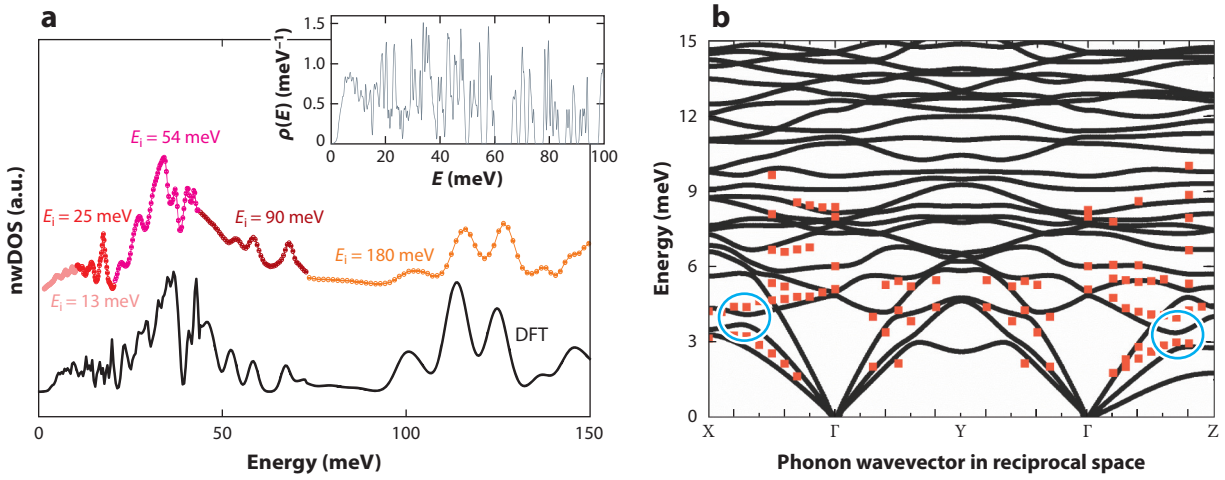

Figure 6

(*a*) Neutron-weighted phonon density of states (nwDOS) of the first dysprosocenium single-molecule magnet [Dy(Cp^tBu_3)$_2$], measured by inelastic neutron scattering (INS) (*colored dots*) and calculated by density-functional theory (DFT) (*black line*). The inset shows the total phonon DOS calculated with DFT. Panel adapted from Reference 42 (CC BY 4.0). (*b*) Phonon dispersion curves for [VO(acetylacetate)$_2$] calculated with DFT (*black lines*) and measured with INS (*red dots*); blue circles show avoided crossings between acoustic and optical modes. The letters on the x-axis represent special positions within the first Brillouin zone. Panel adapted from Reference 129 (CC BY 4.0).

of probing gamma point phonons, nuclear resonant vibrational spectroscopy (NRVS) has recently been shown to be an excellent method capable of directly measuring element-specific vibrations (125). Here, Scherthan, Powell, Schünemann, and coworkers (125) used a synchrotron source to measure NRVS for a Dy(III) SMM, which allowed direct evaluation of phonon modes involving motion of the Dy nucleus—modes that are very likely to be most important in spin–phonon coupling. However, one of the most useful techniques to experimentally probe the phonon DOS is inelastic neutron scattering (INS). INS spectroscopy, in principle, allows for experimental access to phonons of all wave vectors, subject to instrumental limitations. While the use of INS to probe the phonon DOS of materials is widespread, its use in molecular magnetism has been more focused on exploring magnetic transitions (126–128). However, Mills, Chilton, Caretta, and coworkers have recently demonstrated its utility to probe the phonon DOS of the first dysprosocenium SMM and shown that periodic DFT calculations (see below) provide an excellent approximation of the data (42) (**Figure 6*a***). The catch for INS measurements of the phonon DOS is that the data are weighted by the neutron scattering cross section of each nucleus and hence direct access to the DOS is not available; as such, corresponding first-principles calculations are still required to make this leap (**Figure 6*a***). Indeed, going beyond the phonon DOS, one would ideally like to directly measure the phonon dispersion, but this is a significant challenge for molecular crystals, which are often hard to grow large enough for single-crystal INS experiments. However, this exact feat has recently been achieved by Guidi, Sessoli, Carretta, and coworkers (129), who used an aligned array of 40 single crystals to measure the dispersion curves of a V(IV) molecular qubit, [VO(acetylacetate)$_2$]. Their results show excellent agreement with DFT calculations of phonon dispersion curves (**Figure 6*b***), and their analysis is further supplemented by first-principles calculation of the spin–phonon coupling to show how avoided crossings between low-energy optical and acoustic modes induce transfer of strong spin–phonon coupling from the flat optical modes to the dispersive acoustic modes, which has implications for magnetic relaxation at low temperatures.

Regarding the second challenge, measurements most often reveal only the result of spin–phonon coupling (e.g., measurement of T_1 times in SMMs or molecular qubits), and direct probing of the underlying interactions is much rarer. Quite recently, however, there has been some success in employing ultrafast spectroscopy to probe spin–phonon coupling in magnetic molecules more directly. Johansson and coworkers (130) have employed ultrafast transient absorption measurements to show that d-d excitations in a trinuclear Mn(III) SMM are coherently coupled to the in-phase asymmetric stretch along the Jahn-Teller axis, suggesting that optical control of spins in SMMs might be possible. On the other hand, McCusker and coworkers (131) have used ultrafast spectroscopy to characterize the metal-to-ligand charge transfer dynamics in an Fe(II) chromophore and then chemically modified the molecule to inhibit the vibrational modes involved, yielding a chromophore with an MLCT lifetime enhanced by more than an order of magnitude. Although this demonstrates that chemical control of spin–phonon coupling is possible and that it can be employed to deliver improved properties, it remains to be seen how far chemical interventions can be taken to improve spin relaxation properties in molecular magnets.

Aside from ultrafast experiments, a more traditional method to measure the steady-state coupling is with far infrared magnetospectroscopy (FIRMS). This is more-or-less a standard Fourier-transform IR spectrum measured as a function of magnetic field (132). The very small shifts in the IR absorption bands as a function of field must arise due to either spin–phonon transitions or pure electronic transitions, as only the electronic degrees of freedom have a field dependence. Such measurements have been employed to good effect to measure the spin–phonon coupling in magnetic molecules; much of this research has involved the group led by Xue (133–135) as well as from van Slageren and coworkers (136). Recently, Piligkos, Hill, Chilton, and coworkers (137) have used FIRMS to measure and a combination of DFT and CASSCF methods to calculate the spin–phonon coupling in a Yb(III)-based molecular qubit, [Yb(trensal)] [where H_3trensal = 2,2,2-tris(salicylideneimino)trimethylamine], finding excellent agreement between experiment and theory (**Figure 7*a*,*b***). This is an important step beyond standard modeling of FIRMS data to determine spin–phonon coupling and allowed the authors to show that the spectra are subject to an envelope effect whereby only spin–phonon excitations near pure electronic transitions have large intensity (**Figure 7*c***), while the underlying spin–phonon coupling strength is significant across all energy ranges (**Figure 7*d***). Thus, it is crucial when interpreting FIRMS spectra not to assume that only the observed transitions have significant spin–phonon coupling.

Regarding the third challenge, calculation of the spin–phonon coupling is hard because phonons obey quantum mechanics, and hence the nuclear degrees of freedom of a set of atoms should technically be treated in a full many-body quantum framework along with electronic degrees of freedom. While there are theoretical approaches that go to this limit (138), and certainly strong spin–phonon interactions are a crucial ingredient of conventional superconductivity (139), the most common starting point is to separate the nuclear and electronic wave functions via the Born-Oppenheimer approximation. This implicitly assumes the weak spin–phonon coupling limit, which is hoped to be valid for molecular materials. Then, the challenge becomes twofold: (*a*) calculation of the phonon modes themselves and (*b*) determination of how each phonon mode perturbs the electronic states of the molecules (140). For (*a*), first-principles determination of phonon modes most often employs periodic DFT, where a plane-wave ansatz is used to describe the valence electron wave functions of the molecules and effective core potentials describe the core electrons (141). This facilitates the treatment of entire unit cells of molecular crystals and accommodates the use of the Bloch theorem to account for periodicity (142); such techniques have been employed in the solid state to great effect, for instance, in driving innovations in perovskite photovoltaics (143). Indeed, excellent agreement between DFT-calculated and experimental phonon data has been observed for molecular magnets (42, 129), but there is still room for improvement

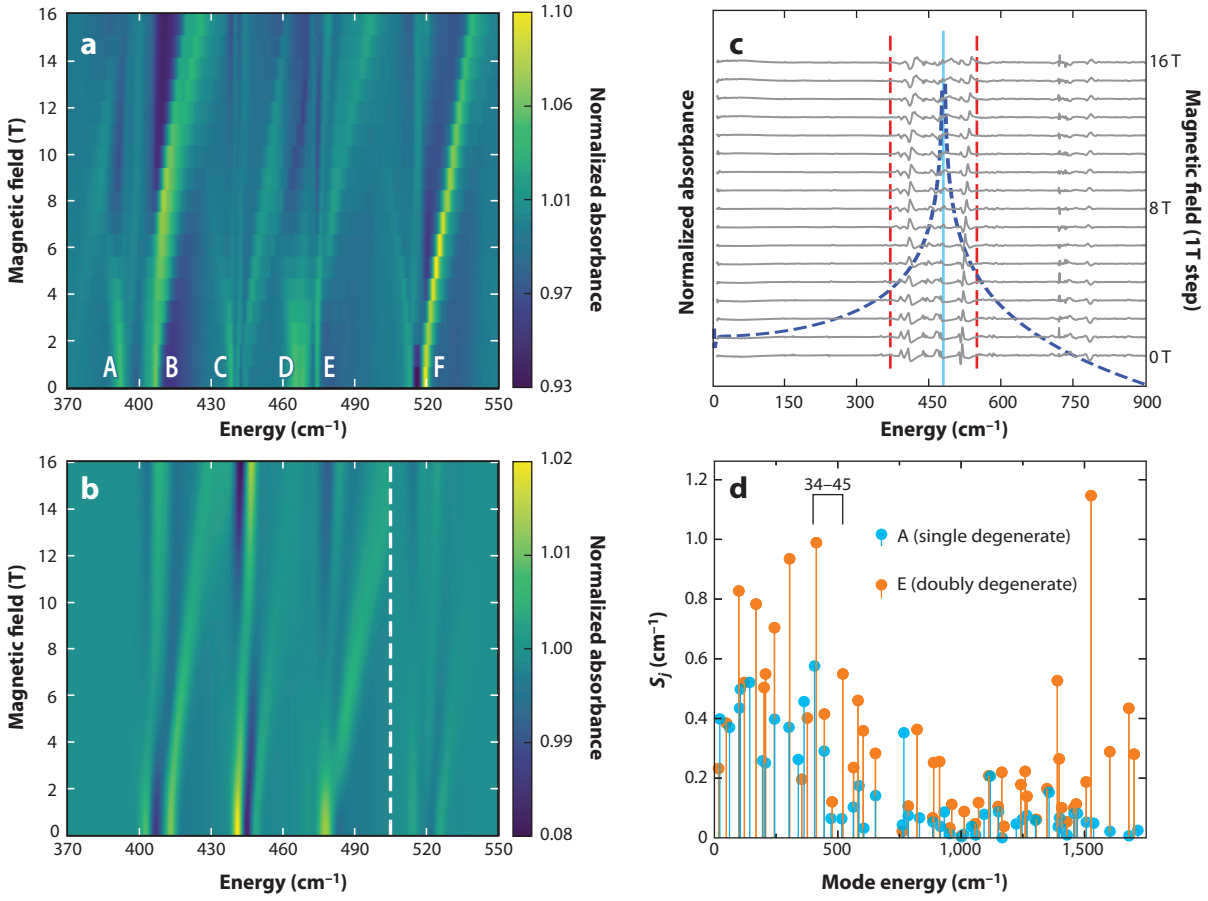

Figure 7

(*a*) Experimental and (*b*) calculated far infrared magnetospectroscopy maps of [Yb(trensal)] in the 370–550 cm^{-1} region. (*c*) Fourier-transform infrared spectra for [Yb(trensal)] as a function of magnetic field, normalized by dividing each spectrum by the average spectrum across all fields, showing field-dependent signals in a small window around 450 cm^{-1} (features around 750 cm^{-1} also have field dependence but are obscured by instrumental artifacts). The light blue solid line shows the position of the experimentally determined first electronic excitation at 474 cm^{-1}, the red dotted lines delineate the region of field dependence in the experimental spectra, and the dark blue dotted line shows the expected envelope for intra-Kramers doublet spin–phonon transitions around the first electronic excited state from first-order perturbation theory. (*d*) Calculated spin–phonon coupling strength for vibrational modes in [Yb(trensal)]. The 34–45 label indicates the transitions observed in panels *a* and *b*. Figure adapted from Reference 137 (CC BY 4.0).

in the treatment of the weak van der Waals interactions in molecular crystals (129) that is crucial for determining the low-energy phonon spectrum. Nonetheless, the accuracy of DFT for calculation of phonons is sufficient in many cases to use as the basis of first-principles calculation of the spin–phonon coupling. Once vibrational properties are known, (*b*) is then a task of scale: For each phononic degree of freedom, of which there can be between 10^2 and 10^4 for molecular crystals, the ways in which the electronic Hamiltonian is modulated needs to be determined. Most often this is done via CASSCF-type calculations (32, 39, 41, 144–147), but there has been exploration of using semiempirical schemes (148) and deploying machine learning algorithms (149) to greatly reduce the computational burden. These calculations are then recast in the form of a model Hamiltonian (see Section 4), which enables the identification of spin–phonon coupling coefficients in a given

model framework; usually this is a CF Hamiltonian for 4f ions (e.g., Equation 3,

$$\hat{H}_{SP-\mathrm{elec}} = \sum_{2\le k\le 2J}^{\mathrm{even}} \sum_{q=-k}^{k} \left(\frac{\partial B_k^q}{\partial Q_j}\right)_{\mathrm{eq}} \hat{O}_k^q, \qquad 3.$$

where the derivatives of the CF parameters as a function of each vibrational normal mode coordinate Q_j are the spin–phonon coupling coefficients) (41) and the ZFS and Zeeman Hamiltonian for 3d ions (144). With these coefficients in hand, it is possible to simulate experimental data such as spin-lattice relaxation T_1 times for SMMs (32, 39, 41, 150) and qubits (88, 145–147), as well as FIRMS maps (137). Indeed, the agreement between experiment and theory appears to be at the level where predictions can be reliably made for new and improved molecular magnets (41).

This section concludes with a few comments on relaxation via QTM. QTM has been thoroughly described for the original 3d-based SMMs (50), where mixing between m_S states of opposing projections due to low-symmetry CF perturbations generates avoided crossings leading to magnetic relaxation via adiabatic passage. However, such avoided crossings cannot occur in a zero magnetic field for Dy(III) SMMs owing to Kramers' theorem. Hence, extrinsic factors must be invoked to describe the presence of QTM; the most common candidates are transverse dipolar magnetic fields and hyperfine coupling. The impact of dipolar fields can be investigated by means of magnetic dilution experiments (most studies of SMMs these days include such a comparison), and the impact of hyperfine coupling can be probed with isotopic enrichment (57, 151–153). However, even when both components are suppressed to some extent, the QTM in Dy(III) SMMs is not quenched (57). Zheng, Liddle, Mills, Chilton, and coworkers (57, 154) have proposed that the spin–phonon coupling plays a role in QTM once Kramers degeneracy is broken by an extrinsic perturbation (such as a dipolar or hyperfine field, neither of which can be completely removed). This has some support from theoretical studies (155), but there is certainly much work to be done to explain why QTM is so prevalent in 4f SMMs with half-integer spin.

6. CONCLUSIONS AND OUTLOOK

This article gives only a brief overview of the field of molecular magnetism. While the focus of this review is on the subtopics of SMMs and molecular qubits, the breadth of activity in the field is astounding, ranging from biochemistry to fundamental physics. In all these areas, however, the structural and spin dynamics of molecular magnets are currently in the spotlight. Here, there is a demand for more focus on the molecule–environment interaction via experimental, theoretical, and computational means. In particular, the crucial role of the spin–phonon coupling has been highlighted, and unraveling the details of this interaction and learning how it can be controlled with chemistry is a big challenge, as is understanding how and why Kramers-conjugate electronic states of the best-performing SMMs are so affected by QTM. On the other hand, considering molecular spin qubits, there has been astounding progress in designing molecules with long coherence times. But now the challenge is to make more practical advances involving coupling and switching of arrays of qubits, and subsequently, further demonstrations of quantum algorithms running on molecular hardware should be a central goal.

DISCLOSURE STATEMENT

The authors are not aware of any affiliations, memberships, funding, or financial holdings that might be perceived as affecting the objectivity of this review.

ACKNOWLEDGMENTS

The author thanks The University of Manchester, the Royal Society (for a University Research Fellowship, URF191320), the European Research Council (ERC-2019-STG-851504), and colleagues past and present for support. Special thanks also go to Dr. Alice Bowen and Mr. Jon Kragskow for assistance.

LITERATURE CITED

1. Harriman KLM, Errulat D, Murugesu M. 2019. Magnetic axiality: design principles from molecules to materials. *Trends Chem.* 1(4):425–39
2. Clérac R, Miyasaka H, Yamashita M, Coulon C. 2002. Evidence for single-chain magnet behavior in a Mn^{III}–Ni^{II} chain designed with high spin magnetic units: a route to high temperature metastable magnets. *J. Am. Chem. Soc.* 124(43):12837–44
3. Pedersen KS, Perlepe P, Aubrey ML, Woodruff DN, Reyes-Lillo SE, et al. 2018. Formation of the layered conductive magnet $CrCl_2(pyrazine)_2$ through redox-active coordination chemistry. *Nat. Chem.* 10(10):1056–61
4. Chen W-P, Singleton J, Qin L, Camón A, Engelhardt L, et al. 2018. Quantum Monte Carlo simulations of a giant $\{Ni_{21}Gd_{20}\}$ cage with a $S = 91$ spin ground state. *Nat. Commun.* 9:2107
5. Kahn O. 1996. Spin-crossover molecular materials. *Curr. Opin. Solid State Mater. Sci.* 1(4):547–54
6. Boča R, Herchel R. 2010. Antisymmetric exchange in polynuclear metal complexes. *Coord. Chem. Rev.* 254(23):2973–3025
7. Lu G, Liu Y, Deng W, Huang G-Z, Chen Y-C, et al. 2020. A perfect triangular dysprosium single-molecule magnet with virtually antiparallel Ising-like anisotropy. *Inorg. Chem. Front.* 7(16):2941–48
8. Chibotaru LF, Ungur L, Soncini A. 2008. The origin of nonmagnetic Kramers doublets in the ground state of dysprosium triangles: evidence for a toroidal magnetic moment. *Angew. Chem. Int. Ed.* 47(22):4126–29
9. Baker ML, Guidi T, Carretta S, Ollivier J, Mutka H, et al. 2012. Spin dynamics of molecular nanomagnets unravelled at atomic scale by four-dimensional inelastic neutron scattering. *Nat. Phys.* 8(12):906–11
10. Ghirri A, Chiesa A, Carretta S, Troiani F, van Tol J, et al. 2015. Coherent spin dynamics in molecular Cr_8Zn wheels. *J. Phys. Chem. Lett.* 6(24):5062–66
11. Ardavan A, Rival O, Morton JJL, Blundell SJ, Tyryshkin AM, et al. 2007. Will spin-relaxation times in molecular magnets permit quantum information processing? *Phys. Rev. Lett.* 98(5):057201
12. Bertaina S, Gambarelli S, Mitra T, Tsukerblat B, Müller A, Barbara B. 2008. Quantum oscillations in a molecular magnet. *Nature* 453(7192):203–6
13. Sessoli R. 2017. Materials science: magnetic molecules back in the race. *Nature* 548(7668):400–1
14. Gaita-Ariño A, Luis F, Hill S, Coronado E. 2019. Molecular spins for quantum computation. *Nat. Chem.* 11(4):301–9
15. Bogani L, Wernsdorfer W. 2008. Molecular spintronics using single-molecule magnets. *Nat. Mater.* 7(3):179–86
16. Parker D, Suturina EA, Kuprov I, Chilton NF. 2020. How the ligand field in lanthanide coordination complexes determines magnetic susceptibility anisotropy, paramagnetic NMR shift, and relaxation behavior. *Acc. Chem. Res.* 53(8):1520–34
17. Perlepe P, Oyarzabal I, Mailman A, Yquel M, Platunov M, et al. 2020. Metal-organic magnets with large coercivity and ordering temperatures up to 242°C. *Science* 370(6516):587–92
18. Caneschi A, Gatteschi D, Sessoli R. 1991. Alternating current susceptibility, high field magnetization, and millimeter band EPR evidence for a ground $S = 10$ state in $[Mn_{12}O_{12}(CH_3COO)_{16}(H_2O)_4]\cdot 2CH_3COOH\cdot 4H_2O$. *J. Am. Chem. Soc.* 113:5873–74
19. Sessoli R, Gatteschi D, Caneschi A, Novak MA. 1993. Magnetic bistability in a metal-ion cluster. *Nature* 365:141–43
20. Sessoli R, Tsai H-L, Schake AR, Wang S, Vincent JB, et al. 1993. High-spin molecules: $[Mn_{12}O_{12}(O_2CR)_{16}(H_2O)_4]$. *J. Am. Chem. Soc.* 115:1804–16

21. Bagai R, Christou G. 2009. The *Drosophila* of single-molecule magnetism: $[Mn_{12}O_{12}(O_2CR)_{16}(H_2O)_4]$. *Chem. Soc. Rev.* 38(4):1011–26
22. Villain J, Hartman-Boutron F, Sessoli R, Rettori A. 1994. Magnetic relaxation in big magnetic molecules. *Europhys. Lett.* 27(2):159–64
23. Ishikawa N, Sugita M, Ishikawa T, Koshihara S, Kaizu Y. 2003. Lanthanide double-decker complexes functioning as magnets at the single-molecular level. *J. Am. Chem. Soc.* 125(29):8694–95
24. Woodruff DN, Winpenny REP, Layfield RA. 2013. Lanthanide single-molecule magnets. *Chem. Rev.* 113(7):5110–48
25. Abragam A, Bleaney B. 1970. *Electron Paramagnetic Resonance of Transition Ions*. Oxford, UK: Oxford Univ. Press
26. Rinehart JD, Long JR. 2011. Exploiting single-ion anisotropy in the design of f-element single-molecule magnets. *Chem. Sci.* 2(11):2078–85
27. Sievers J. 1982. Asphericity of 4f-shells in their Hund's rule ground states. *Z. Phys. B Condens. Matter* 45(4):289–96
28. Chilton NF, Collison D, McInnes EJL, Winpenny REP, Soncini A. 2013. An electrostatic model for the determination of magnetic anisotropy in dysprosium complexes. *Nat. Commun.* 4:2551
29. Chilton NF, Goodwin CAP, Mills DP, Winpenny REP. 2015. The first near-linear bis(amide) f-block complex: a blueprint for a high temperature single molecule magnet. *Chem. Commun.* 51(1):101–3
30. Chilton NF. 2015. Design criteria for high-temperature single-molecule magnets. *Inorg. Chem.* 54(5):2097–99
31. Giansiracusa MJ, Kostopoulos AK, Collison D, Winpenny REP, Chilton NF. 2019. Correlating blocking temperatures with relaxation mechanisms in monometallic single-molecule magnets with high energy barriers ($U_{eff} > 600$ K). *Chem. Commun.* 55:7025–28
32. Goodwin CAP, Ortu F, Reta D, Chilton NF, Mills DP. 2017. Molecular magnetic hysteresis at 60 kelvin in dysprosocenium. *Nature* 548(7668):439–42
33. Day BM, Guo F-S, Layfield RA. 2018. Cyclopentadienyl ligands in lanthanide single-molecule magnets: one ring to rule them all? *Acc. Chem. Res.* 51(8):1880–89
34. Demir S, Zadrozny JM, Long JR. 2014. Large spin-relaxation barriers for the low-symmetry organolanthanide complexes $[Cp^*_2Ln(BPh_4)]$ (Cp^* = pentamethylcyclopentadienyl; Ln = Tb, Dy). *Chem. Eur. J.* 20(31):9524–29
35. Meng Y-S, Zhang Y-Q, Wang Z-M, Wang B-W, Gao S. 2016. Weak ligand-field effect from ancillary ligands on enhancing single-ion magnet performance. *Chem. Eur. J.* 22(36):12724–31
36. Demir S, Boshart MD, Corbey JF, Woen DH, Gonzalez MI, et al. 2017. Slow magnetic relaxation in a dysprosium ammonia metallocene complex. *Inorg. Chem.* 56(24):15049–56
37. McClain KR, Gould CA, Chakarawet K, Teat S, Groshens TJ, et al. 2018. High-temperature magnetic blocking and magneto-structural correlations in a series of dysprosium(III) metallocenium single-molecule magnets. *Chem. Sci.* 9:8492–503
38. Guo F-S, Day BM, Chen Y-C, Tong M-L, Mansikkamäki A, Layfield RA. 2018. Magnetic hysteresis up to 80 kelvin in a dysprosium metallocene single-molecule magnet. *Science* 362(6421):1400–3
39. Evans P, Reta D, Whitehead GFS, Chilton NF, Mills DP. 2019. Bis-monophospholyl dysprosium cation showing magnetic hysteresis at 48 K. *J. Am. Chem. Soc.* 141(50):19935–40
40. Gould CA, McClain KR, Yu JM, Groshens TJ, Furche F, et al. 2019. Synthesis and magnetism of neutral, linear metallocene complexes of terbium(II) and dysprosium(II). *J. Am. Chem. Soc.* 141(33):12967–73
41. Reta D, Kragskow JGC, Chilton NF. 2021. Ab initio prediction of high-temperature magnetic relaxation rates in single-molecule magnets. *J. Am. Chem. Soc.* 143(15):5943–50
42. Chiesa A, Cugini F, Hussain R, Macaluso E, Allodi G, et al. 2020. Understanding magnetic relaxation in single-ion magnets with high blocking temperature. *Phys. Rev. B* 101(17):174402
43. Sessoli R, Gatteschi D, Caneschi A, Novak MA. 1993. Magnetic bistability in a metal-ion cluster. *Nature* 365:141–43
44. Ganivet CR, Ballesteros B, de la Torre G, Clemente-Juan JM, Coronado E, Torres T. 2013. Influence of peripheral substitution on the magnetic behavior of single-ion magnets based on homo- and heteroleptic Tb^{III} bis(phthalocyaninate). *Chem. Eur. J.* 19(4):1457–65

45. Ding Y-S, Chilton NF, Winpenny REP, Zheng Y-Z. 2016. On approaching the limit of molecular magnetic anisotropy: a near-perfect pentagonal bipyramidal dysprosium(III) single-molecule magnet. *Angew. Chem. Int. Ed.* 55(52):16071–74
46. Gould CA, McClain KR, Reta D, Kragskow JGC, Marchiori DA, et al. 2022. Ultrahard magnetism from mixed-valence dilanthanide complexes with metal-metal bonding. *Science* 375(6577):198–202
47. Giansiracusa MJ, Al-Badran S, Kostopoulos AK, Whitehead GFS, Collison D, et al. 2019. A large barrier single-molecule magnet without magnetic memory. *Dalton Trans.* 48(29):10795–98
48. Escalera-Moreno L, Baldoví JJ, Gaita-Ariño A, Coronado E. 2018. Spin states, vibrations and spin relaxation in molecular nanomagnets and spin qubits: a critical perspective. *Chem. Sci.* 9(13):3265–75
49. Friedman JR, Sarachik MP, Tejada J, Ziolo R. 1996. Macroscopic measurement of resonant magnetization tunneling in high-spin molecules. *Phys. Rev. Lett.* 76(20):3830–33
50. Garanin DA, Chudnovsky EM. 1997. Thermally activated resonant magnetization tunneling in molecular magnets: $Mn_{12}Ac$ and others. *Phys. Rev. B* 56(17):11102–18
51. Giansiracusa MJ, Moreno-Pineda E, Hussain R, Marx R, Martínez Prada M, et al. 2018. Measurement of magnetic exchange in asymmetric lanthanide dimetallics: toward a transferable theoretical framework. *J. Am. Chem. Soc.* 140(7):2504–13
52. Blagg RJ, Ungur L, Tuna F, Speak J, Comar P, et al. 2013. Magnetic relaxation pathways in lanthanide single-molecule magnets. *Nat. Chem.* 5(8):673–78
53. Demir S, Jeon I-R, Long JR, Harris TD. 2015. Radical ligand-containing single-molecule magnets. *Coord. Chem. Rev.* 289–290:149–76
54. Rinehart JD, Fang M, Evans WJ, Long JR. 2011. A N_2^{3-} radical-bridged terbium complex exhibiting magnetic hysteresis at 14 K. *J. Am. Chem. Soc.* 133(36):14236–39
55. Demir S, Gonzalez MI, Darago LE, Evans WJ, Long JR. 2017. Giant coercivity and high magnetic blocking temperatures for N_2^{3-} radical-bridged dilanthanide complexes upon ligand dissociation. *Nat. Commun.* 8(1):2144
56. Liu J-L, Chen Y-C, Tong M-L. 2018. Symmetry strategies for high performance lanthanide-based single-molecule magnets. *Chem. Soc. Rev.* 47(7):2431–53
57. Ortu F, Reta D, Ding Y-S, Goodwin CAP, Gregson MP, et al. 2019. Studies of hysteresis and quantum tunnelling of the magnetisation in dysprosium(III) single molecule magnets. *Dalton Trans.* 48(24):8541–45
58. Demir S, Zadrozny JM, Nippe M, Long JR. 2012. Exchange coupling and magnetic blocking in bipyrimidyl radical-bridged dilanthanide complexes. *J. Am. Chem. Soc.* 134(45):18546–49
59. Gould CA, Darago LE, Gonzalez MI, Demir S, Long JR. 2017. A trinuclear radical-bridged lanthanide single-molecule magnet. *Angew. Chem. Int. Ed.* 56(34):10103–7
60. Liu F, Krylov DS, Spree L, Avdoshenko SM, Samoylova NA, et al. 2017. Single molecule magnet with an unpaired electron trapped between two lanthanide ions inside a fullerene. *Nat. Commun.* 8:16098
61. DiVincenzo DP. 2000. The physical implementation of quantum computation. *Fortschr. Phys.* 48(9–11):771–83
62. Hahn EL. 1950. Spin echoes. *Phys. Rev.* 80(4):580–94
63. Bader K, Dengler D, Lenz S, Endeward B, Jiang S-D, et al. 2014. Room temperature quantum coherence in a potential molecular qubit. *Nat. Commun.* 5:5304
64. Atzori M, Tesi L, Morra E, Chiesa M, Sorace L, Sessoli R. 2016. Room-temperature quantum coherence and rabi oscillations in vanadyl phthalocyanine: toward multifunctional molecular spin qubits. *J. Am. Chem. Soc.* 138(7):2154–57
65. Ariciu A-M, Woen DH, Huh DN, Nodaraki LE, Kostopoulos AK, et al. 2019. Engineering electronic structure to prolong relaxation times in molecular qubits by minimising orbital angular momentum. *Nat. Commun.* 10(1):3330
66. Zadrozny JM, Niklas J, Poluektov OG, Freedman DE. 2015. Millisecond coherence time in a tunable molecular electronic spin qubit. *ACS Cent. Sci.* 1(9):488–92
67. Balasubramanian G, Neumann P, Twitchen D, Markham M, Kolesov R, et al. 2009. Ultralong spin coherence time in isotopically engineered diamond. *Nat. Mater.* 8(5):383–87
68. Miao KC, Blanton JP, Anderson CP, Bourassa A, Crook AL, et al. 2020. Universal coherence protection in a solid-state spin qubit. *Science* 396(6510):1493–97

69. Whitehead GFS, Moro F, Timco GA, Wernsdorfer W, Teat SJ, Winpenny REP. 2013. A ring of rings and other multicomponent assemblies of cages. *Angew. Chem. Int. Ed.* 52(38):9932–35
70. Fernandez A, Ferrando-Soria J, Pineda EM, Tuna F, Vitorica-Yrezabal IJ, et al. 2016. Making hybrid [*n*]-rotaxanes as supramolecular arrays of molecular electron spin qubits. *Nat. Commun.* 7:10240
71. Zadrozny JM, Gallagher AT, Harris TD, Freedman DE. 2017. A porous array of clock qubits. *J. Am. Chem. Soc.* 139(20):7089–94
72. Yamabayashi T, Atzori M, Tesi L, Cosquer G, Santanni F, et al. 2018. Scaling up electronic spin qubits into a three-dimensional metal-organic framework. *J. Am. Chem. Soc.* 140(38):12090–101
73. Yu C-J, von Kugelgen S, Krzyaniak MD, Ji W, Dichtel WR, et al. 2020. Spin and phonon design in modular arrays of molecular qubits. *Chem. Mater.* 32(23):10200–206
74. Moreno-Pineda E, Godfrin C, Balestro F, Wernsdorfer W, Ruben M. 2018. Molecular spin qudits for quantum algorithms. *Chem. Soc. Rev.* 47(2):501–13
75. Aguilà D, Barrios LA, Velasco V, Roubeau O, Repollés A, et al. 2014. Heterodimetallic [LnLn′] lanthanide complexes: toward a chemical design of two-qubit molecular spin quantum gates. *J. Am. Chem. Soc.* 136(40):14215–22
76. Atzori M, Chiesa A, Morra E, Chiesa M, Sorace L, et al. 2018. A two-qubit molecular architecture for electron-mediated nuclear quantum simulation. *Chem. Sci.* 9(29):6183–92
77. Luis F, Alonso PJ, Roubeau O, Velasco V, Zueco D, et al. 2020. A dissymmetric [Gd_2] coordination molecular dimer hosting six addressable spin qubits. *Commun. Chem.* 3:176
78. Macaluso E, Rubín M, Aguilà D, Chiesa A, Barrios LA, et al. 2020. A heterometallic [LnLn′Ln] lanthanide complex as a qubit with embedded quantum error correction. *Chem. Sci.* 11:10337–43
79. Wasielewski MR, Forbes MDE, Frank NL, Kowalski K, Scholes GD, et al. 2020. Exploiting chemistry and molecular systems for quantum information science. *Nat. Rev. Chem.* 4(9):490–504
80. Yu C-J, von Kugelgen S, Laorenza DW, Freedman DE. 2021. A molecular approach to quantum sensing. *ACS Cent. Sci.* 7(5):712–23
81. Awschalom DD, Hanson R, Wrachtrup J, Zhou BB. 2018. Quantum technologies with optically interfaced solid-state spins. *Nat. Photon.* 12(9):516–27
82. Bayliss SL, Laorenza DW, Mintun PJ, Kovos BD, Freedman DE, Awschalom DD. 2020. Optically addressable molecular spins for quantum information processing. *Science* 370(6522):1309–12
83. Mabbs FE, Machin DJ. 1973. *Magnetism and Transition Metal Complexes*. London: Chapman and Hall
84. Fataftah MS, Bayliss SL, Laorenza DW, Wang X, Phelan BT, et al. 2020. Trigonal bipyramidal V^{3+} complex as an optically addressable molecular qubit candidate. *J. Am. Chem. Soc.* 142(48):20400–8
85. Shiddiq M, Komijani D, Duan Y, Gaita-Ariño A, Coronado E, Hill S. 2016. Enhancing coherence in molecular spin qubits via atomic clock transitions. *Nature* 531(7594):348–51
86. Bollinger JJ, Prestage JD, Itano WM, Wineland DJ. 1985. Laser-cooled-atomic frequency standard. *Phys. Rev. Lett.* 54(10):1000–3
87. Kundu K, White JRK, Moehring SA, Yu JM, Ziller JW, et al. 2021. Clock transition due to a record 1240 G hyperfine interaction in a Lu(II) molecular spin qubit. ChemRxiv. **https://doi.org/10.26434/chemrxiv.14399333.v1**
88. Atzori M, Tesi L, Benci S, Lunghi A, Righini R, et al. 2017. Spin dynamics and low energy vibrations: insights from vanadyl-based potential molecular qubits. *J. Am. Chem. Soc.* 139(12):4338–41
89. Atzori M, Benci S, Morra E, Tesi L, Chiesa M, et al. 2018. Structural effects on the spin dynamics of potential molecular qubits. *Inorg. Chem.* 57(2):731–40
90. Santanni F, Albino A, Atzori M, Ranieri D, Salvadori E, et al. 2021. Probing vibrational symmetry effects and nuclear spin economy principles in molecular spin qubits. *Inorg. Chem.* 60(1):140–51
91. Bayliss SL, Laorenza DW, Mintun PJ, Kovos BD, Freedman DE, Awschalom DD. 2020. Optically addressable molecular spins for quantum information processing. *Science* 370(6522):1309–12
92. Shiddiq M, Komijani D, Duan Y, Gaita-Ariño A, Coronado E, Hill S. 2016. Enhancing coherence in molecular spin qubits via atomic clock transitions. *Nature* 531:348–51
93. Vincent R, Klyatskaya S, Ruben M, Wernsdorfer W, Balestro F. 2012. Electronic read-out of a single nuclear spin using a molecular spin transistor. *Nature* 488:357–60
94. Candini A, Klyatskaya S, Ruben M, Wernsdorfer W, Affronte M. 2011. Graphene spintronic devices with molecular nanomagnets. *Nano Lett.* 11(7):2634–39

95. Urdampilleta M, Klyatskaya S, Cleuziou J-P, Ruben M, Wernsdorfer W. 2011. Supramolecular spin valves. *Nat. Mater.* 10(7):502–6
96. Deleted in proof
97. Thiele S, Balestro F, Ballou R, Klyatskaya S, Ruben M, Wernsdorfer W. 2014. Electrically driven nuclear spin resonance in single-molecule magnets. *Science* 344(6188):1135–38
98. Godfrin C, Ferhat A, Ballou R, Klyatskaya S, Ruben M, et al. 2017. Operating quantum states in single magnetic molecules: implementation of Grover's quantum algorithm. *Phys. Rev. Lett.* 119(18):187702
99. Koike N, Uekusa H, Ohashi Y, Harnoode C, Kitamura F, et al. 1996. Relationship between the skew angle and interplanar distance in four bis(phthalocyaninato)lanthanide(III) tetrabutylammonium salts ($[NBu^n_4][Ln^{III}Pc_2]$; Ln = Nd, Gd, Ho, Lu). *Inorg. Chem.* 35(20):5798–804
100. Molloy KC. 2013. Ferrocene. In *Group Theory for Chemists*, ed. K Molloy, pp. 109–18. Cambridge, UK: Woodhead Publ. 2nd ed.
101. Robin MB, Day P. 1968. Mixed valence chemistry-a survey and classification. In *Advances in Inorganic Chemistry and Radiochemistry*, Vol. 10, ed. HJ Emeléus, AG Sharpe, pp. 247–422. New York: Academic
102. Edelstein NM, Allen PG, Bucher JJ, Shuh DK, Sofield CD, et al. 1996. The oxidation state of Ce in the sandwich molecule cerocene. *J. Am. Chem. Soc.* 118(51):13115–16
103. Kerridge A, Kaltsoyannis N. 2010. All-electron CASPT2 study of $Ce(\eta^8\text{–}C_8H_6)_2$. *C. R. Chim.* 13(6):853–59
104. MacDonald MR, Bates JE, Ziller JW, Furche F, Evans WJ. 2013. Completing the series of +2 ions for the lanthanide elements: synthesis of molecular complexes of Pr^{2+}, Gd^{2+}, Tb^{2+}, and Lu^{2+}. *J. Am. Chem. Soc.* 135(26):9857–68
105. Meihaus KR, Fieser ME, Corbey JF, Evans WJ, Long JR. 2015. Record high single-ion magnetic moments through $4f^n5d^1$ electron configurations in the divalent lanthanide complexes $[(C_5H_4SiMe_3)_3Ln]$. *J. Am. Chem. Soc.* 137(31):9855–60
106. Slater JC. 1929. The theory of complex spectra. *Phys. Rev.* 34(10):1293–322
107. Condon EU. 1930. The theory of complex spectra. *Phys. Rev.* 36(7):1121–33
108. Racah G. 1942. Theory of complex spectra. I. *Phys. Rev.* 61(3–4):186–97
109. Racah G. 1942. Theory of complex spectra. II. *Phys. Rev.* 62(9–10):438–62
110. Bethe H. 1929. Termaufspaltung in Kristallen. *Ann. Phys.* 395(2):133–208
111. Figgis BN, Hitchman MA. 1999. *Ligand Field Theory and Its Applications*. New York: Wiley-VCH. 1st ed.
112. Mulak J, Gajek Z. 2000. *The Effective Crystal Field Potential*. Oxford, UK: Elsevier
113. Ryabov I. 2009. On the operator equivalents and the crystal-field and spin Hamiltonian parameters. *Appl. Magn. Reson.* 35(3):481–94
114. Rudowicz C, Sung HWF. 2001. Can the electron magnetic resonance (EMR) techniques measure the crystal (ligand) field parameters? *Phys. B Condens. Matter* 300(1):1–26
115. Stoll S, Schweiger A. 2006. EasySpin, a comprehensive software package for spectral simulation and analysis in EPR. *J. Magn. Reson.* 178(1):42–55
116. Speldrich M, Schilder H, Lueken H, Kögerler P. 2011. A computational framework for magnetic polyoxometalates and molecular spin structures: CONDON 2.0. *Isr. J. Chem.* 51(2):215–27
117. Chilton NF, Anderson RP, Turner LD, Soncini A, Murray KS. 2013. PHI: a powerful new program for the analysis of anisotropic monomeric and exchange-coupled polynuclear d- and f-block complexes. *J. Comput. Chem.* 34(13):1164–75
118. Roos BO, Taylor PR, Sigbahn PEM. 1980. A complete active space SCF method (CASSCF) using a density matrix formulated super-CI approach. *Chem. Phys.* 48(2):157–73
119. Ungur L, Chibotaru LF. 2015. Computational modelling of the magnetic properties of lanthanide compounds. In *Lanthanides and Actinides in Molecular Magnetism*, ed. RA Layfield, M Murugesu, pp. 153–84. Weinheim, Ger.: Wiley-VCH
120. Anisimov VI, Zaanen J, Andersen OK. 1991. Band theory and Mott insulators: Hubbard *U* instead of Stoner *I*. *Phys. Rev. B* 44(3):943–54
121. Liechtenstein AI, Anisimov VI, Zaanen J. 1995. Density-functional theory and strong interactions: orbital ordering in Mott-Hubbard insulators. *Phys. Rev. B* 52(8):R5467–70
122. Stein CJ, von Burg V, Reiher M. 2016. The delicate balance of static and dynamic electron correlation. *J. Chem. Theory Comput.* 12(8):3764–73

123. Andersson K, Malmqvist P-Å, Roos BO, Sadlej AJ, Wolinski K. 1990. Second-order perturbation theory with a CASSCF reference function. *J. Phys. Chem.* 94(14):5483–88
124. Angeli C, Cimiraglia R, Evangelisti S, Leininger T, Malrieu J-P. 2001. Introduction of *n*-electron valence states for multireference perturbation theory. *J. Chem. Phys.* 114(23):10252–64
125. Scherthan L, Pfleger RF, Auerbach H, Hochdörffer T, Wolny JA, et al. 2020. Exploring the vibrational side of spin-phonon coupling in single-molecule magnets via ^{161}Dy nuclear resonance vibrational spectroscopy. *Angew. Chem. Int. Ed.* 59(23):8818–22
126. Waldmann O, Güdel H. 2005. Many-spin effects in inelastic neutron scattering and electron paramagnetic resonance of molecular nanomagnets. *Phys. Rev. B* 72(9):094422
127. Stavretis SE, Atanasov M, Podlesnyak AA, Hunter SC, Neese F, Xue Z-L. 2015. Magnetic transitions in iron porphyrin halides by inelastic neutron scattering and ab initio studies of zero-field splittings. *Inorg. Chem.* 54(20):9790–801
128. Vonci M, Giansiracusa MJ, Gable RW, den Heuvel WV, Latham K, et al. 2015. Ab initio calculations as a quantitative tool in the inelastic neutron scattering study of a single-molecule magnet analogue. *Chem. Commun.* 52:2091–94
129. Garlatti E, Tesi L, Lunghi A, Atzori M, Voneshen DJ, et al. 2020. Unveiling phonons in a molecular qubit with four-dimensional inelastic neutron scattering and density functional theory. *Nat. Commun.* 11(1):1751
130. Liedy F, Eng J, McNab R, Inglis R, Penfold TJ, et al. 2020. Vibrational coherences in manganese single-molecule magnets after ultrafast photoexcitation. *Nat. Chem.* 12(5):452–58
131. Paulus BC, Adelman SL, Jamula LL, McCusker JK. 2020. Leveraging excited-state coherence for synthetic control of ultrafast dynamics. *Nature* 582(7811):214–18
132. Fishman RS. 2018. *Spin-Wave Theory and Its Applications to Neutron Scattering and THz Spectroscopy*. Bristol, UK: IOP Publ.
133. Moseley DH, Stavretis SE, Thirunavukkuarasu K, Ozerov M, Cheng Y, et al. 2018. Spin-phonon couplings in transition metal complexes with slow magnetic relaxation. *Nat. Commun.* 9(1):2572
134. Stavretis SE, Moseley DH, Fei F, Cui H, Cheng Y, et al. 2019. Spectroscopic studies of the magnetic excitation and spin-phonon couplings in a single-molecule magnet. *Chem. Eur. J.* 25(69):15846–57
135. Moseley DH, Stavretis SE, Zhu Z, Guo M, Brown CM, et al. 2020. Inter-Kramers transitions and spin-phonon couplings in a lanthanide-based single-molecule magnet. *Inorg. Chem.* 59(7):5218–30
136. Rechkemmer Y, Breitgoff FD, van der Meer M, Atanasov M, Hakl M, et al. 2016. A four-coordinate cobalt(II) single-ion magnet with coercivity and a very high energy barrier. *Nat. Commun.* 7:10467
137. Kragskow JGC, Marbey J, Buch CD, Nehrkorn J, Ozerov M, et al. 2022. Analysis of vibronic coupling in a 4f molecular magnet with FIRMS. *Nat. Commun.* 13:825
138. Dresselhaus T, Bungey CBA, Knowles PJ, Manby FR. 2020. Coupling electrons and vibrations in molecular quantum chemistry. *J. Chem. Phys.* 153(21):214114
139. Bardeen J, Cooper LN, Schrieffer JR. 1957. Theory of superconductivity. *Phys. Rev.* 108(5):1175–204
140. Lunghi A, Sanvito S. 2019. How do phonons relax molecular spins? *Sci. Adv.* 5(9):eaax7163
141. Lejaeghere K, Bihlmayer G, Bjorkman T, Blaha P, Blugel S, et al. 2016. Reproducibility in density functional theory calculations of solids. *Science* 351(6280):aad3000
142. Dove MT. 1993. *Introduction to Lattice Dynamics*. Cambridge; UK: Cambridge Univ. Press
143. Frost JM, Butler KT, Brivio F, Hendon CH, van Schilfgaarde M, Walsh A. 2014. Atomistic origins of high-performance in hybrid halide perovskite solar cells. *Nano Lett.* 14(5):2584–90
144. Lunghi A, Totti F, Sessoli R, Sanvito S. 2017. The role of anharmonic phonons in under-barrier spin relaxation of single molecule magnets. *Nat. Commun.* 8:14620
145. Lunghi A, Totti F, Sanvito S, Sessoli R. 2017. Intra-molecular origin of the spin-phonon coupling in slow-relaxing molecular magnets. *Chem. Sci.* 8(9):6051–59
146. Albino A, Benci S, Tesi L, Atzori M, Torre R, et al. 2019. First-principles investigation of spin-phonon coupling in vanadium-based molecular spin quantum bits. *Inorg. Chem.* 58(15):10260–68
147. Escalera-Moreno L, Suaud N, Gaita-Ariño A, Coronado E. 2017. Determining key local vibrations in the relaxation of molecular spin qubits and single-molecule magnets. *J. Phys. Chem. Lett.* 8:1695–700

148. Escalera-Moreno L, Baldoví JJ, Gaita-Ariño A, Coronado E. 2020. Design of high-temperature *f*-block molecular nanomagnets through the control of vibration-induced spin relaxation. *Chem. Sci.* 11(6):1593–98
149. Lunghi A, Sanvito S. 2020. The limit of spin lifetime in solid-state electronic spins. *J. Phys. Chem. Lett.* 11(15):6273–78
150. Yu K-X, Kragskow JGC, Ding Y-S, Zhai Y-Q, Reta D, et al. 2020. Enhancing magnetic hysteresis in single-molecule magnets by ligand functionalization. *Chemistry* 6(7):1777–93
151. Moreno-Pineda E, Damjanović M, Fuhr O, Wernsdorfer W, Ruben M. 2017. Nuclear spin isomers: engineering a $Et_4N[DyPc_2]$ spin qudit. *Angew. Chem. Int. Ed.* 56(33):9915–19
152. Pointillart F, Bernot K, Golhen S, Le Guennic B, Guizouarn T, et al. 2015. Magnetic memory in an isotopically enriched and magnetically isolated mononuclear dysprosium complex. *Angew. Chem. Int. Ed.* 54(5):1504–7
153. Kishi Y, Pointillart F, Lefeuvre B, Riobé F, Guennic BL, et al. 2017. Isotopically enriched polymorphs of dysprosium single molecule magnets. *Chem. Commun.* 53(25):3575–78
154. Ding Y-S, Yu K-X, Reta D, Ortu F, Winpenny REP, et al. 2018. Field- and temperature-dependent quantum tunnelling of the magnetisation in a large barrier single-molecule magnet. *Nat. Commun.* 9(1):3134
155. Irländer K, Schnack J. 2020. Spin-phonon interaction induces tunnel splitting in single-molecule magnets. *Phys. Rev. B* 102(5):054407